Mutations of *ADAMTS9* Cause Nephronophthisis-Related Ciliopathy

Yo Jun Choi,[1] Jan Halbritter,[2,3] Daniela A. Braun,[2] Markus Schueler,[2] David Schapiro,[2] John Hoon Rim,[1] Sumeda Nandadasa,[4] Won-il Choi,[2] Eugen Widmeier,[2] Shirlee Shril,[2] Friederike Körber,[5] Sidharth K. Sethi,[6] Richard P. Lifton,[7,8] Bodo B. Beck,[9,10,11] Suneel S. Apte,[4] Heon Yung Gee,[1,*] and Friedhelm Hildebrandt[2,*]

Nephronophthisis-related ciliopathies (NPHP-RCs) are a group of inherited diseases that are associated with defects in primary cilium structure and function. To identify genes mutated in NPHP-RC, we performed homozygosity mapping and whole-exome sequencing for >100 individuals, some of whom were single affected individuals born to consanguineous parents and some of whom were siblings of indexes who were also affected by NPHP-RC. We then performed high-throughput exon sequencing in a worldwide cohort of 800 additional families affected by NPHP-RC. We identified two *ADAMTS9* mutations (c.4575_4576del [p.Gln1525Hisfs*60] and c.194C>G [p.Thr65Arg]) that appear to cause NPHP-RC. Although ADAMTS9 is known to be a secreted extracellular metalloproteinase, we found that ADAMTS9 localized near the basal bodies of primary cilia in the cytoplasm. Heterologously expressed wild-type ADAMTS9, in contrast to mutant proteins detected in individuals with NPHP-RC, localized to the vicinity of the basal body. Loss of ADAMTS9 resulted in shortened cilia and defective sonic hedgehog signaling. Knockout of *Adamts9* in IMCD3 cells, followed by spheroid induction, resulted in defective lumen formation, which was rescued by an overexpression of wild-type, but not of mutant, ADAMTS9. Knockdown of *adamts9* in zebrafish recapitulated NPHP-RC phenotypes, including renal cysts and hydrocephalus. These findings suggest that the identified mutations in *ADAMTS9* cause NPHP-RC and that ADAMTS9 is required for the formation and function of primary cilia.

Introduction

Nephronophthisis (NPHP [MIM: 256100]) is the most frequent genetic cause of chronic renal failure in children. Histologically, NPHP is characterized by the development of massive interstitial fibrosis with abnormal thickness of the tubular basement membranes, and in later stages, the formation of cysts that are mainly distributed at the cortico-medullary junction.[1] Some affected individuals with NPHP also present with extrarenal symptoms, including retinitis pigmentosa, intellectual disability, cerebellar ataxia, bone anomalies, or liver fibrosis. These syndromes, referred to as NPHP-related ciliopathies (NPHP-RCs), are clinically and genetically heterogeneous disorders that cause dysplastic or degenerative diseases in the kidney, liver, retina, and central nervous system.[1]

NPHP-RCs result from defects in primary cilia, which are sensory cilia that are generally non-motile, are present on most cells in vertebrates, and control key signaling pathways during development and tissue homeostasis.[2] More than 90 different genes have been identified as monogenic recessive causes of NPHP-RC if mutated.[3] Depending on the composition of the examined cohort, mutations in these genes account for 50%–60% of NPHP-RC cases.[4,5] Most of the encoded proteins participate in functional protein subcomplexes that participate in multiple signaling mechanisms and localize to the primary cilia, centrosomes, mitotic spindle, or abscission structures in a cell-cycle-dependent manner.[3]

Because the genetic and molecular basis of 40%–50% of NPHP-RC cases is unsolved, we applied homozygosity mapping and whole-exome sequencing to >100 affected individuals born of consanguineous parents or siblings of index individuals who were also affected by NPHP-RC in order to identify additional single-gene causes of NHPH-RC. From these methods, in combination with high-throughput exon sequencing in a cohort of 800 individuals with NPHP-RC, we identified recessive mutations in *ADAMTS9* as a cause of NPHP-RC. We demonstrate that ADAMTS9 localizes near the basal body of the primary cilium and is required for proper ciliary function.

Material and Methods

Research Subjects

Blood samples and pedigrees were obtained from individuals with diagnosed NPHP-RC after informed consent was provided. Approval for human-subject research was obtained from the

[1]Department of Pharmacology, Brain Korea 21 PLUS Project for Medical Sciences, Yonsei University College of Medicine, Seoul 03722, Korea; [2]Division of Nephrology, Department of Medicine, Boston Children's Hospital, Harvard Medical School, Boston, MA 02115, USA; [3]Division of Nephrology, Department of Internal Medicine, University Hospital Leipzig, Leipzig 04103, Germany; [4]Department of Biomedical Engineering, Cleveland Clinic Lerner Research Institute, Cleveland, OH 44195, USA; [5]Department of Radiology, University Hospital Cologne, Cologne 50931, Germany; [6]Kidney Institute, Medanta, the Medicity, Gurgaon, Haryana 122001, India; [7]Department of Genetics, Yale University School of Medicine, New Haven, CT 06510, USA; [8]Laboratory of Human Genetics and Genomics, Rockefeller University, New York, NY 10065, USA; [9]Institute of Human Genetics, University Hospital Cologne, Cologne 50931, Germany; [10]Center for Molecular Medicine Cologne, Cologne 50931, Germany; [11]Center for Rare and Hereditary Kidney Disease Cologne, Cologne 50931, Germany
*Correspondence: hygee@yuhs.ac (H.Y.G.), friedhelm.hildebrandt@childrens.harvard.edu (F.H.)
https://doi.org/10.1016/j.ajhg.2018.11.003.

institutional review boards of the University of Michigan and Boston Children's Hospital.

Linkage Analysis

For genome-wide homozygosity mapping, the GeneChip Human Mapping 250k *Sty*I Array from Affymetrix was used. Nonparametric logarithm of the odds (LOD) scores were calculated via a modified version of the program GENEHUNTER 2.1[6,7] through stepwise use of a sliding window with sets of 110 SNPs. The program ALLEGRO[8] was used for identifying regions of homozygosity as previously described;[9] a disease allele frequency of 0.0001 and Caucasian marker allele frequencies were specified.

Whole-Exome Sequencing

Whole-exome sequencing (WES) was performed via Agilent SureSelect human exome capture arrays and next-generation sequencing (NGS) was performed on the Illumina sequencing platform. Sequence reads were mapped against the human reference genome (NCBI build 37 [UCSC hg19]) in CLC Genomics Workbench (version 9.0.1) software (QIAGEN). Variant calling and filtering were performed as previously described.[10]

High-Throughput Mutation Analysis by Array-Based Multiplex PCR and NGS

A cohort of 800 individuals with NPHP-RC was sequenced in batches of 48 DNA samples at a time; 672 amplicons (592 exons) from approximately 30 candidate genes, including *ADAMTS9*, were sequenced via the PCR-based 48.48 Access Array microfluidic technology (Fluidigm) and consecutive NGS as previously described.[11] Detected variants were confirmed by Sanger sequencing and evaluated for segregation.

Plasmid Construction and Site-Directed Mutagenesis

The cDNA for human *ADAMTS9* was purchased from OriGene Technologies and was subcloned into the pENTR-D-TOPO vector (Invitrogen). Expression vectors were created with LR clonase (Invitrogen) according to the manufacturer's instructions. Clones reflecting the *ADAMTS9* mutations that were identified in individuals with NPHP-RC were introduced into the cDNA constructs in the pENTR-D-TOPO vector with a QuikChange II XL site-directed mutagenesis kit (Agilent Technologies).

Cell Culture and Transfection

Mouse inner medullary collecting duct-3 (IMCD3, CRL-2123) and hTERT retinal pigment epithelial-1 (RPE1, CRL-4000) cells were obtained from the American Type Culture Collection (ATCC) and cultured in DMEM/F12 with 10% fetal bovine serum (FBS) and penicillin (50 IU/mL) and streptomycin (50 μg/mL). *ADAMTS9*-specific and control-scrambled short interfering RNAs (siRNAs) were purchased from Dharmacon. The siRNAs were transfected into RPE1 cells via MISSION siRNA transfection reagent (Sigma). So that *Adamts9* knockout (KO) could be achieved, IMCD3 cells were transduced with lentivirus containing lentiCRISPR v2 (Addgene plasmid #52961), and transformants were selected and maintained with 4 mg/mL puromycin. The target sequences of siRNAs and single guide RNAs (sgRNAs) used in this study are shown in Table S1. Human fibroblasts and mouse embryonic fibroblasts were grown in DMEM supplemented with 15% FBS, penicillin (50 IU/mL) and streptomycin (50 μg/mL), and non-essential amino acids (Invitrogen). Human embryonic kidney 293 (HEK293) cells were cultured in DMEM supplemented with 10% FBS and penicillin (50 IU/ml) and streptomycin (50 μg/ml) (Invitrogen). The cells were transfected with plasmids via Lipofectamine and PLUS reagent, or Lipofectamine 2000 (Invitrogen), according to the manufacturer's instructions.

Immunoblotting and Immunofluorescence

Anti-ADAMTS9 (Novus, NBP1-82916), anti-β-actin (Abcam, ab6276), anti-γ-tubulin (Abcam, ab11316), anti-acetylated-α-tubulin (Abcam, ab24610), anti-Myc (Santa Cruz Biotechnology, sc-40 and sc-789), anti-acetylated-α-tubulin (Sigma, T7451), anti-GLI1 (Cell Signaling Technology, #2534), and anti-GLI3 (R&D Systems, AF3690) antibodies were obtained from commercial sources. Alexa 488-, Alexa-594-, and Alexa-647-conjugated secondary antibodies and DAPI (4′,6-diamidino-2-phenylindole dihydrochloride) were obtained from Invitrogen. HRP-labeled secondary antibodies were purchased from Santa Cruz Biotechnology. Confocal images were obtained with a Carl Zeiss LSM780 microscope or Leica SP5X system with an DM6000 upright compound microscope. Image processing and analysis were performed with the ZEN or Leica AF suite. For immunofluorescence, IMCD3 or RPE1 cells were seeded at a low density and grown to 80% confluence. For ciliation analysis, IMCD3 or RPE1 cells were grown to confluence and then starved of serum for 48 hr.

Scanning Electron Microscopy

The cells were fixed with 2% glutaraldehyde-paraformaldehyde in 0.1 M phosphate buffer (pH 7.4) for 6 hr and washed two times for 30 min each with 0.1 M phosphate buffer. They were post-fixed for 1.5 hr with 1% OsO_4 that was dissolved in 0.1 M phosphate buffer. Then, cells were dehydrated in an ascending, gradual series (50%–100%) of ethanol, and samples were treated with isoamyl acetate and subjected to a critical-point dryer (Leica EM CPD300). They were coated with platinum (5 nm) by an ion coater (Leica EM ACE600) and examined with a scanning electron microscope (Carl Zeiss FE-SEM) at 7 kV.

Real-Time PCR

RNA samples were isolated from RPE1 cells with RiboEx (GeneAll Biotechnology) and reverse-transcribed with an iScript cDNA Synthesis Kit (Bio-Rad). Samples were assayed with SYBR Green ready master mix and ROX reference dye (Takara Bio); primers are listed in Table S1. Real-time PCR was performed with the StepOnePlus Real-Time PCR System (Applied Biosystems). The relative RNA expression levels were calculated via a comparative threshold cycle (Ct) method that used glyceraldehyde 3-phosphate dehydrogenase (*GAPDH*) as a control.

Spheroid Assay

Spheroid assays were performed as previously described.[12] Control and *Adamts9* KO IMCD3 cells were trypsinized, and resuspended cells were then mixed 1:1 with growth-factor-reduced Geltrx (GIBCO) and seeded on a Nunc Lab-Tek II chambered coverglass (Thermo Fisher). After 72 hr, the cells were stained and imaged with a Zeiss LSM700 confocal microscope, which identified spheroids with visible cleared lumens. For rescue experiments, IMCD3 cells were transfected with human *ADAMTS9* cDNA constructs and, after 24 hr, were trypsinized. In each spheroid, nuclei were counted.

Rearing Zebrafish Embryos and Microinjecting Morpholinos and mRNA

Approval for zebrafish (*Danio rerio*) research was obtained from the University Committee on the Use and Care of Animals (UCUCA) of the Boston Children's Hospital and Yonsei University College of Medicine. Wild-type zebrafish embryos were obtained from natural spawnings of AB-line fish and raised at 28.5°C. A standard control and *adamts9* morpholinos (MOs) were designed and purchased from Gene Tools. Fertilized eggs were microinjected at the 1- to 2-cell stage with 0.2 mM MOs diluted in 200 mM KCl, 0.1% phenol red (Sigma-Aldrich), and 10 mM HEPES. The scoring of cyst formation and zebrafish embryo imaging were conducted on mixed male and female embryos 48 hr after fertilization under a Leica MZ16 stereo microscope. For histological analysis, zebrafish embryos were fixed with 4% paraformaldehyde overnight at 4°C; dehydrated with an ethanol series of 25%, 50%, 75%, and 95% ethanol; and equilibrated with JB-4 solution (Polysciences) overnight at 4°C. The zebrafish embryos were then embedded in JB-4 resin and sectioned with a Leica R2265 microtome. The 6 μm sections were then stained with methylene blue.

Statistical Analysis

The results are presented as the means ± standard deviation for the indicated number of experiments. Statistical analysis of continuous data was performed with two-tailed Student's t tests. $p < 0.05$ was considered statistically significant.

Results

ADAMTS9 Mutations Cause NPHP-RC

In order to identify additional genes mutated in NPHP-RC, we performed homozygosity mapping and WES in >100 consanguineous individuals or siblings of index individuals who were also affected with NPHP-RC. One child of European origin (F1279-21) was 5 years of age and had end-stage renal disease (ESRD) from NPHP and phenotypes characteristic of Joubert syndrome (MIM: 213300); such phenotypes included corpus callosum hypoplasia and aplasia of the vermis (Figures 1A–1C and Table 1). In addition, individual F1279-21 presented with proteinuria, deafness, atrial septal defects, coloboma, and short stature (Table 1). Homozygosity mapping yielded four regions of homozygosity by descent; these regions had a cumulative genomic length of 104.9 Mb and represented candidate regions for a recessive mutation (Figure 1D). WES detected a homozygous truncating mutation (c.4575_4576del [p.Gln1525Hisfs*60]) in *ADAMTS9* (a disintegrin-like and metalloproteinase with thrombospondin motifs 9 [MIM: 605421] [GenBank: NM_182920.1]) (Table 1 and Figure 1E). In more than 90 genes analyzed in this individual, no likely pathogenic mutation with a known connection to NPHP-RC was found. In the gnomAD database, there are 53 predicted loss-of-function alleles for *ADAMTS9*; however, their minor-allele frequencies are less than 0.0005, and there are no homozygotes for any of these alleles.

To discover additional mutations in *ADAMTS9*, we performed high-throughput exon sequencing in a worldwide cohort of 800 additional families affected by NPHP-RC.[4,11] We detected a homozygous missense variant (c.194C>G [p.Thr65Arg]) in *ADAMTS9* in an Arabic child (A5048-21) from consanguineous parents (Table 1 and Figure 1F). We additionally performed WES of individual A5048-21 and excluded mutations in genes previously linked to NPHP-RC. Homozygosity mapping of this individual yielded 24 homozygosity segments, which had a cumulative genomic length of 263 Mb (Figure 1G); *ADAMTS9* was within one of these segments, on chromosome 3. The variant (c.194C>G [p.Thr65Arg]) in *ADAMTS9* is reported as a SNP in the dbSNP database; however, its minor-allele frequency is 0.0002, and it does not appear in the homozygous state in the gnomAD database (Table 1). In addition, multiple tools have predicted it to be deleterious for protein function, and it alters an amino-acid residue that is evolutionarily conserved from humans down to *Caenorhabditis elegans* (Table 1 and Figure S1A). Individual A5048-21 showed increased echogenicity on ultrasound (Figure 1H) and had proteinuria, deafness, hepatosplenomegaly, anemia, thrombocytopenia, short stature, and osteopenia and had had ESRD due to NPHP since infancy (Table 1).

ADAMTS9 was previously identified as a positive regulator of ciliogenesis in a genome-wide screen performed in RPE1 cells through the use of siRNAs.[13] In addition, the orientation of primary cilia is perturbed in umbilical-artery smooth-muscle cells in mice with a hypomorphic *Adamts9* allele (*Adamts9*^{Gt}).[14] However, the functional relationship of ADAMTS9 to primary cilia has not been well established.

ADAMTS9 Localizes Near Basal Bodies of Primary Cilia

Because NPHP-RC proteins localize to primary cilia, centrosomes, mitotic spindles, and abscission structures at various stages in the cell cycle,[2] we first examined the localization of ADAMTS9 in cell lines with primary cilia. Interestingly, ADAMTS9 was detected near the basal bodies of primary cilia during interphase in human dermal fibroblasts, RPE1 cells, mouse embryonic fibroblasts, and IMCD3 cells (Figure 2A). In addition, ADAMTS9 was also observed in vesicular structures in the cytoplasm of human fibroblasts (Figure 2A, arrows). During mitosis, ADAMTS9 was not observed near centrosomes but was mostly found in cytoplasmic vesicles in IMCD3 cells (Figure S2).

To examine whether exogenous ADAMTS9 can be targeted to basal bodies, we transfected RPE1 cells with C-terminal Myc-tagged ADAMTS9 (ADAMTS9-Myc). When overexpressed, wild-type ADAMTS9, like endogenous ADAMTS9, localized near the base of primary cilia (Figure 2B), whereas neither p.Thr65Arg nor p.Gln1525Hisfs*60 mutant proteins were observed near the basal body (Figures 2C and 2D). We also examined whether these mutations affected secretion of ADAMTS9; however, both mutant proteins, as well as wild-type ADAMTS9 protein, were detected in the culture medium of transfected cells, indicating that the secretion of ADAMTS9 was unaffected by the mutations (Figure S3).

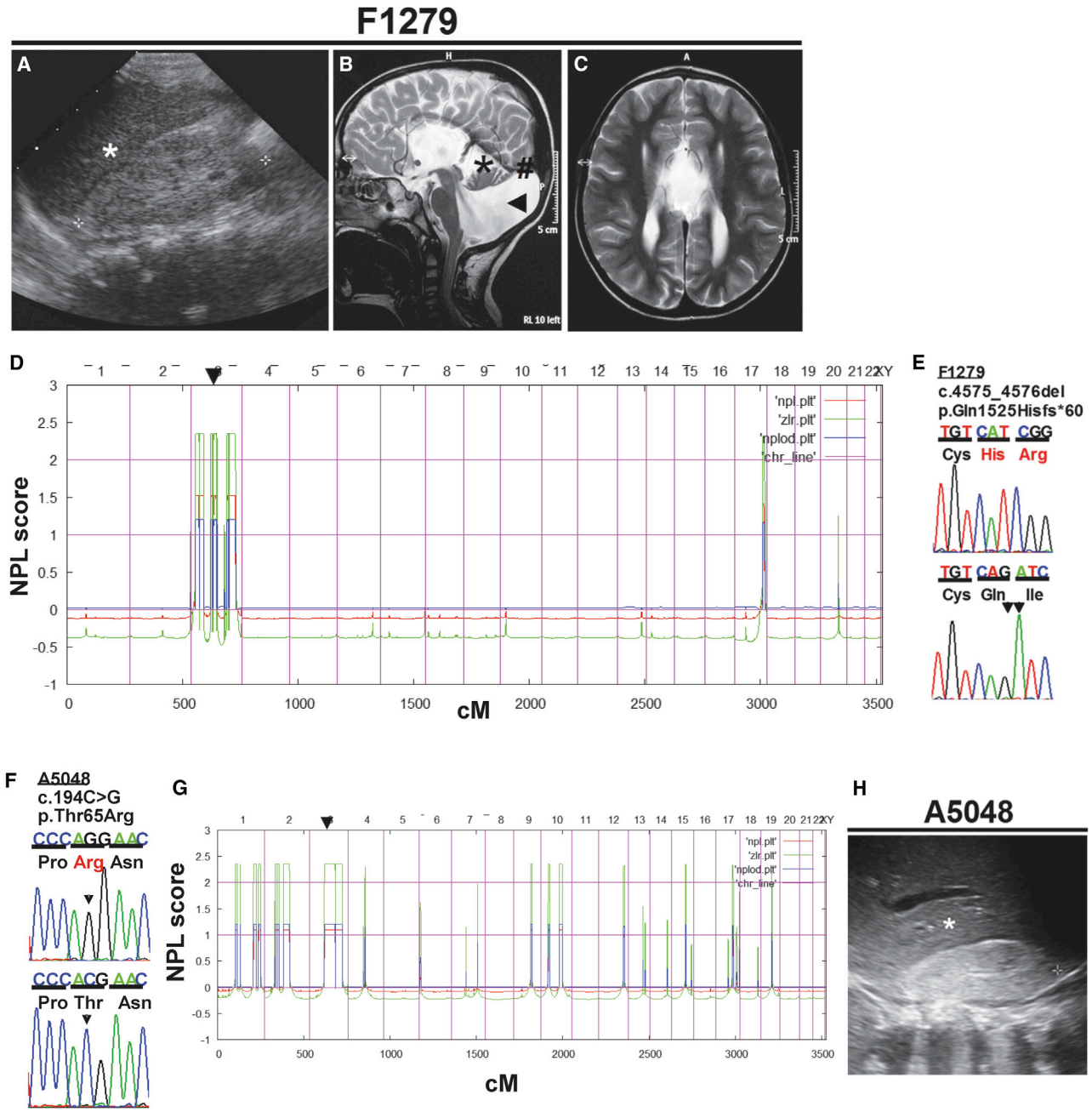

Figure 1. Clinical Findings, Homozygosity Mapping, and Detection of Causative Variants in *ADAMTS9* by Whole-Exome Sequencing in Individuals with NPHP-RC

(A) An ultrasound of individual F1279-21's right kidney shows the organ has increased echogenicity compared to that of his liver (*).
(B–C) Brain MRI of individual F1279-21. The sagittal image shows cystic dilation of the fourth ventricle (arrowhead), cephalad rotation of the vermian remnant (*), and elevation of the torcular herophili and sinus rectus (#) (B). The transverse image demonstrates dysgenesis of the corpus callosum (C).
(D) For individual F1279-21, non-parametric LOD (NPL) scores from homozygosity mapping are plotted across the x axis, which shows Affymetrix 250K *Sty*I array SNP positions on human chromosomes concatenated from pter (left) to qter (right). Genetic distance is given in cM. Note that the *ADAMTS9* locus (arrowhead) is positioned within a maximum NPL peak on chromosome 3p.
(E and F) Sanger sequencing traces show altered nucleotides (arrowheads).
(G) Homozygosity mapping of individual A5048-21.
(H) An ultrasound of individual A5048-21's right kidney shows the organ has increased echogenicity compared to that of his liver (*).

On the basis of these findings, we investigated whether endocytosis of ADAMTS9 after secretion allowed its localization near the basal body. To address this question, we transfected RPE1 cells with the ADAMTS9-Myc construct and treated them with an endocytosis inhibitor, either Dynasore or Pitstop 2. The ciliary localization of ADAMTS9 was not observed after treatment with either inhibitor (Figures 2E–2G). In addition, overexpression of wild-type

Table 1. Mutations of *ADAMTS9* in Two Families with Nephronophthisis-Related Ciliopathies

Family–Individual	Ethnic Origin	Nucleotide Alteration[a]	Deduced Protein change	Exon/Intron (State)	MT	PP2	SIFT	Continuous amino acid sequence conservation	Parental Consanguinity	EVS Frequency	dbSNP	gnomAD Frequency	Renal Manifestation	Renal Biopsy	Extrarenal Manifestation
F1279–21	European	c.4575_4576del	p.Gln1525Hisfs*60	30 (hom)	N/A	N/A	N/A	N/A	no	–	–	–	increased echogenicity, medullary cysts, proteinuria, ESRD at 5 yr	ND	cortical deafness, ASD, growth retardation, short stature, coloboma, aplasia of vermis, corpus callosum hypoplasia
A5048–21	Arabic	c.194C>G	p.Thr65Arg	2 (hom)	DC (1.00)	dam (0.559)	del (1.00)	*C. elegans*	yes	GG/GC/CC = 6502/1/0	rs192420947 (MAF, 0.0002)	64/277,230 (0.0002309, no homozygote)	NPHP, nonselective proteinuria, ESRD since infancy	Microcystic dilatation of tubules, immature glomeruli (at 2 yr)	sensorineural deafness, hepatosplenomegaly, short stature, anemia, thrombocytopenia, osteopenia, rickets

Abbreviations are as follows: ASD = atrial septal defect; dam = damaging; DC = disease causing; del = deleterious; ESRD = end-stage renal disease; EVS = Exome Variant Server; gnomAD = Genome Aggregation Database; hom = homozygous; MAF = minor allele frequency; MT = MutationTaster; N/A = not applicable; ND = no data; NPHP = nephronophthisis; PP2 = PolyPhen-2; and SIFT = Sorting Intolerant From Tolerant.
[a]*ADAMTS9* cDNA mutations are numbered according to human cDNA reference sequence NM_182920.1.

dynamin did not affect the localization of ADAMTS9 near the basal body (Figure 2H), whereas this localization was inhibited by overexpression of dominant-negative dynamin (K44A, Figure 2I). These data indicated that endocytosis is required for the localization of ADAMTS9 near the basal bodies.

Loss of ADAMTS9 Results in Defects in Primary Cilia

Because *ADAMTS9* mutations appear to cause NPHP-RC and because ADAMTS9 localizes near the basal bodies of primary cilia, we investigated the effects of ADAMTS9 on ciliogenesis. To do this, we generated IMCD3 cells in which *Adamts9* was knocked out via the CRISPR/Cas9 system (Figure S4A). Two *Adamts9* knockout (KO) cells, KO#1 (c.275_279del [p.Trp92Serfs*2]) and KO#2 (c.269_270del [p.Val90Alafs*5]), were confirmed by Sanger sequencing and immunoblotting (Figures S4B and S4C). Upon serum starvation, *Adamts9* KO cells had shorter primary cilia than control IMCD3 cells (Figures 3A–3C). Scanning electron microscopy also confirmed that knockout of *Adamts9* resulted in shortened primary cilia (Figure 3B). We also knocked down ADAMTS9 in RPE1 cells by using siRNA, and we observed similar but milder defect (Figures S5A–S5C). *Adamts9* KO IMCD3 cells showed a statistically significant reduction in the percentage of ciliated cells compared to control IMCD3 cells (Figure 3D).

Because hedgehog (hh) signaling is mediated through primary cilia[15] and sonic hh (Shh) signaling is defective in *Adamts9*$^{Gt/Gt}$ vascular smooth muscle cells,[14] we examined Shh signaling in RPE1 cells. The translocation of smoothened (SMO) into primary cilia upon Shh pathway activation was investigated through the use of RPE1 cells that stably expressed GFP-tagged SMO. SMO-GFP was observed at the base of primary cilia; however, upon stimulation by SAG (a chlorobenzothiophene-containing compound that acts as a SMO agonist), SMO-GFP signals became stronger and were observed along ciliary axoneme (Figure 3E). When *ADAMTS9* was knocked down by siRNA, the translocation of SMO-GFP into shortened primary cilia was not observed (Figure 3E). The addition of 100 nM SAG to RPE1 cells for 24 hr resulted in increased mRNA amounts of *SMO*, *GLI1*, and *GLI2* in comparison to baseline amounts without SAG stimulation (Figure 3F). In contrast, *ADAMTS9* knockdown with two different siRNAs reduced the upregulation of Shh target genes, indicating defects in the primary cilia (Figure 3F). After ADAMTS9 knockdown by siRNA transfection, we observed decreased GLI1, consistent with the real-time PCR data (Figure 3G). To further confirm a defect in Shh signaling, we measured the levels of the full-length GLI3 (GLI3FL) and repressor (GLI3R) forms. When the Shh ligand is not present, GLI3FL is cleaved into GLI3R, and this cleavage is inhibited by activation of Shh pathways.[16] In control RPE1 cells, SAG treatment reduced the levels of both GLI3FL and GLI3R (Figures 3G and S5D). However, in cells transfected with *ADAMTS9* siRNA, neither the amount of

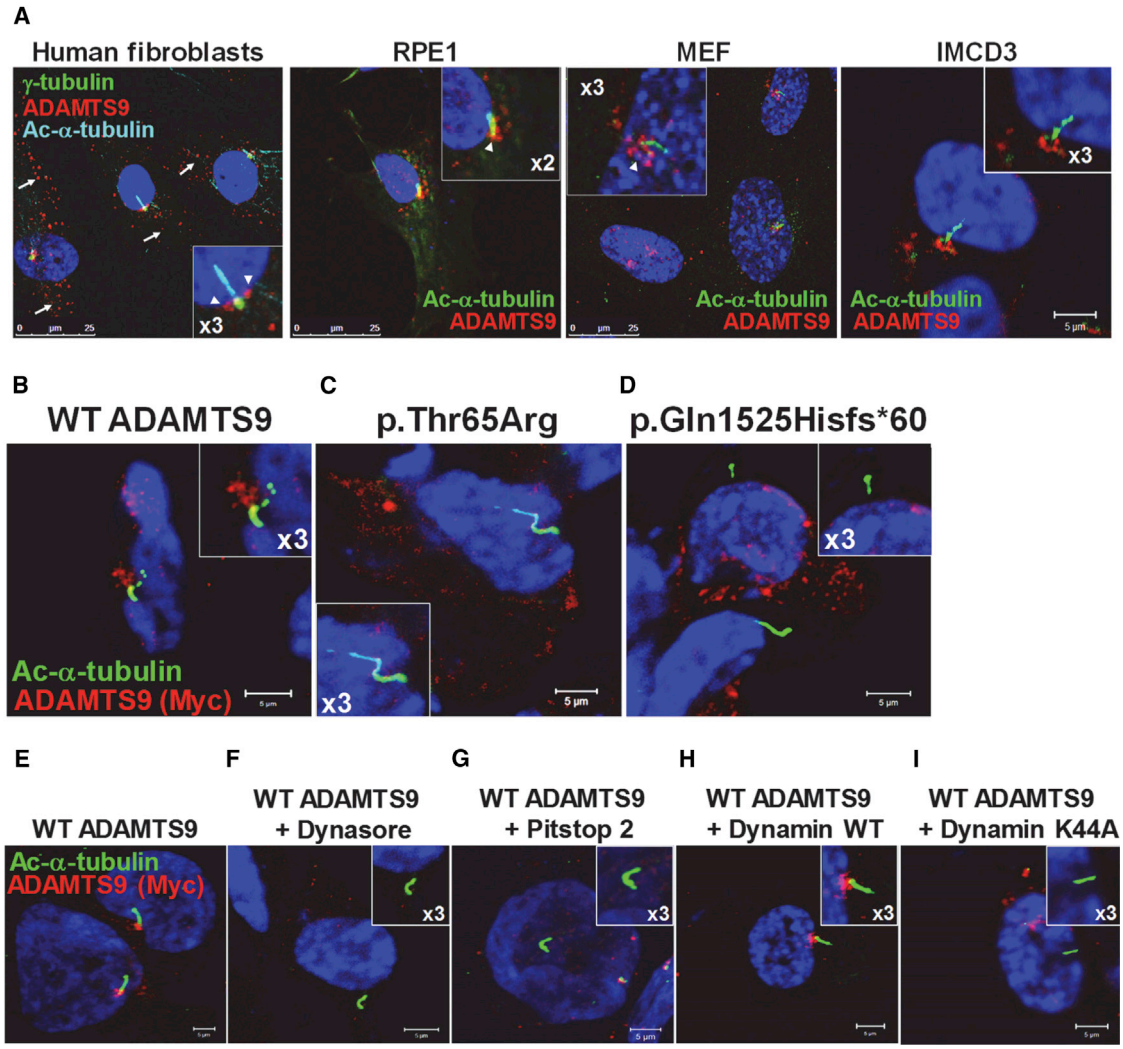

Figure 2. ADAMTS9 Localizes Near the Basal Body of Primary Cilia

(A) Localization of ADAMTS9 in ciliated human dermal fibroblasts, retinal pigment epithelium-1 (RPE1) cells, mouse embryonic fibroblasts (MEFs), and inner medullary collecting duct-3 (IMCD3) cells. Cells were starved of serum for 48 hr so that primary cilium formation would be induced; cells were then stained with anti-ADAMTS9, anti-acetylated-α-tubulin (Ac-α-tubulin), or anti-γ-tubulin antibodies.

(B–D) Localization of exogenous ADAMTS9 in RPE1 cells. RPE1 cells were transfected with C-terminal Myc-tagged wild-type (WT) and mutant *ADAMTS9* cDNA constructs, starved of serum for 48 hr, and then stained with anti-Ac-α-tubulin and anti-Myc antibodies.

(E–I) Effect of endocytosis inhibition on the localization of exogenous WT ADAMTS9 in RPE1 cells. Note that treatment with the endocytosis inhibitors Dynasore (F) or Pitstop 2 (G), or overexpression of dominant-negative Dynamin (K44A) (I), prevented the localization of WT ADAMTS9 near the basal body.

GLI3FL nor that of GLI3R decreased upon SAG treatment (Figures 3G and S5D).

To elucidate the role of ADAMTS9 in the pathogenesis of NPHP-RC, we examined the effects of *Adamts9* KO by using a 3D spheroid model, a well-established model for recapitulating polarity defects seen in NPHP-RC.[12] Control IMCD3 cells developed spheroids with a clear lumen surrounded by a monolayer of cells, apical cilia, and clear apicobasal polarity (Figure 4A). By contrast, *Adamts9* KO IMCD3 cells formed defective spheroids characterized by mislocalized β-catenin at the basolateral membrane and an irregular lumen surrounded by multiple layers of cells (Figures 4B and 4C). This defect could be partially rescued by concurrent transfection with wild-type human *ADAMTS9* (Figure 4D), but not with either *ADAMTS9* mutant (Figures 4E and 4F). Figure 4G shows quantification of these results. Taken together, these findings indicated that the identified mutations induced the loss of the ciliary function of ADAMTS9.

adamts9 Knockdown Replicates Ciliopathy Phenotypes in Zebrafish

To further validate the causative roles of ADAMTS9 mutations in the NPHP-RC phenotypes, we performed knockdown of the *ADAMTS9* ortholog in zebrafish. We used translation-blocking (AUG) and exon 3 splice donor (e3i3) antisense morpholinos (MOs). The efficiency of the e3i3 MO was confirmed by RT-PCR, which demonstrated deletion

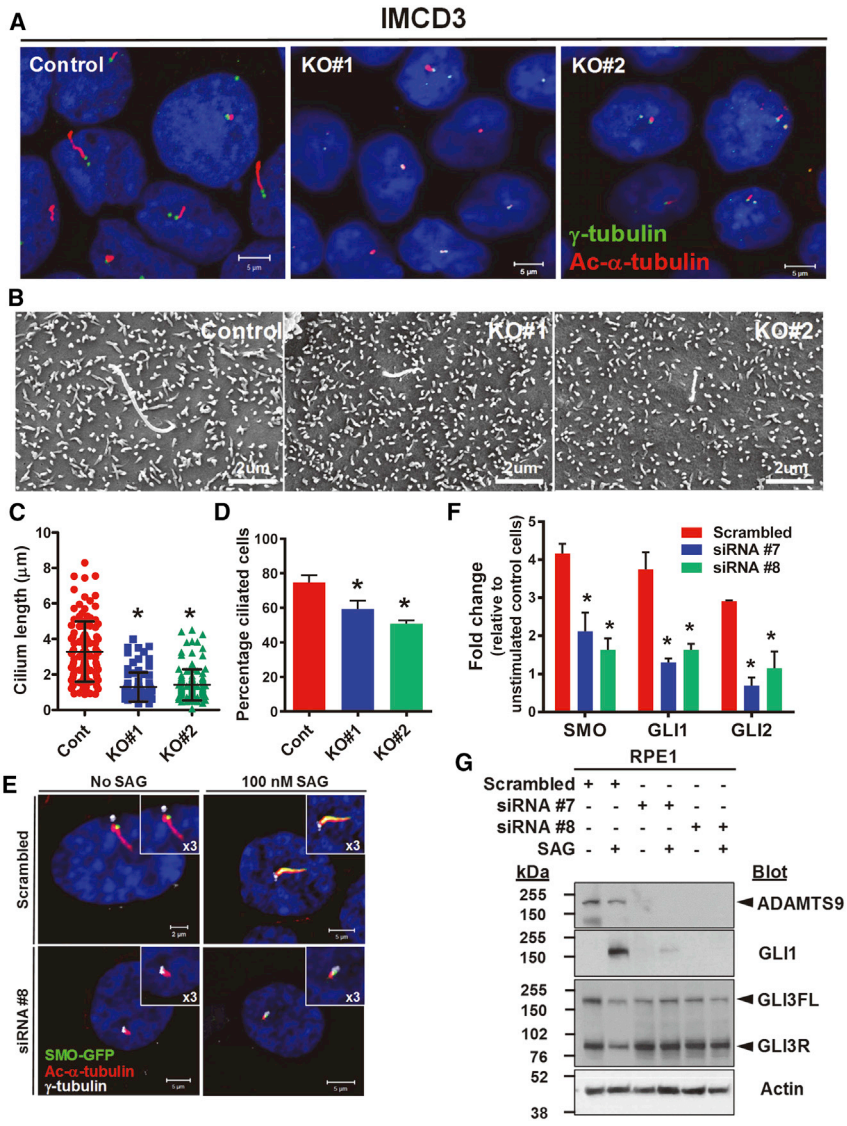

Figure 3. Loss of *ADAMTS9* Causes Defects in Primary Cilia

(A) Effect of *Adamts9* knockout (KO) via the CRISPR/Cas9 system on primary cilia in IMCD3 cells. The length of the primary cilia of IMCD3 cells was shortened by *Adamts9* KO. Cells were starved of serum for 48 hr and then stained with anti-acetylated-α-tubulin (Ac-α-tubulin) and anti-γ-tubulin antibodies.

(B) Scanning-electron-microscopy images of primary cilia from control and *Adamts9* KO cells.

(C) Cilium length was measured on the basis of Ac-α-tubulin staining in >100 cells per condition. *$p < 0.05$, t test.

(D) Percentage of ciliated cells. Experiments were repeated more than three times independently, and more than 100 cells were counted in each experiment. Data represent means ± standard deviation (SD). *$p < 0.05$, t test.

(E) Translocation of SMO into primary cilia is defective upon *ADAMTS9* knockdown by siRNA.

(F) Effects of *ADAMTS9* knockdown on Shh signaling in RPE1 cells. Upon stimulation by 100 nM SMO agonist (SAG), Shh target genes were upregulated in control cells but not in cells treated with siRNAs. Data represent means ±SD of four independent experiments. *$p < 0.05$, t test.

(G) Immunoblot analysis of GLI processing in unstimulated and SAG-stimulated RPE1 cells with and without *ADAMTS9* knockdown.

of exon 3 (Figure 5A). Knockdown of *adamts9* in zebrafish replicated characteristic ciliopathy phenotypes,[17] including a ventrally curved body axis, hydrocephalus, or pronephric cysts at 3 days post-fertilization (dpf) (Figures 5B and 5C). Approximately 60% of morphants showed single or multiple ciliopathy phenotypes (Figure 5D), strongly suggesting that zebrafish *adamts9* also has a role in primary cilium formation and function. Therefore, the role of ADAMTS9 in primary cilia seems to be evolutionarily conserved.

Discussion

In this study, we identified recessive *ADAMTS9* mutations that cause NPHP-RC. ADAMTS9 and a homolog, ADAMTS20, have a striking resemblance to their *C. elegans* ortholog, GON-1.[18–20] These proteases are members of a large secreted zinc metalloprotease family, whose members play diverse roles in tissue morphogenesis and human genetic and acquired conditions.[21] Members of the family share several distinct protein modules, including a propeptide, a metalloproteinase domain, a disintegrin-like domain, and thrombospondin type 1 motifs (Figure S1B).[21] ADAMTS9 and GON-1 share a unique C-terminal domain called the GON-1 domain (Figure S1B).[18] The proteoglycans aggrecan and versican are known substrates of ADAMTS9, and *Adamts9*$^{-/-}$ mice die during early gestation.[22] The two individuals with recessive *ADAMTS9* mutations in this study presented with early-onset ESRD resulting from NPHP; proteinuria; deafness; short stature; and developmental delay. However, some clinical features differed between the two cases; for example, individual F1279-21 had developmental brain defects, but individual A5048-21 did not. Broad pleiotropy is a common feature of NPHP-RC, and mutations in the same gene can give rise to diverse phenotypes depending on the mutated allele.[3] In addition, modifier alleles can influence phenotypic expressivity, such as when retinopathy manifests in individuals who have recessive *NPHP1* mutations and also carry a heterozygous *AHI* mutation.[23] Individual F1279-21 had a homozygous frameshift mutation that resulted in a truncated protein with loss of both several thrombospondin motifs and the GON domain. In light of the fact that

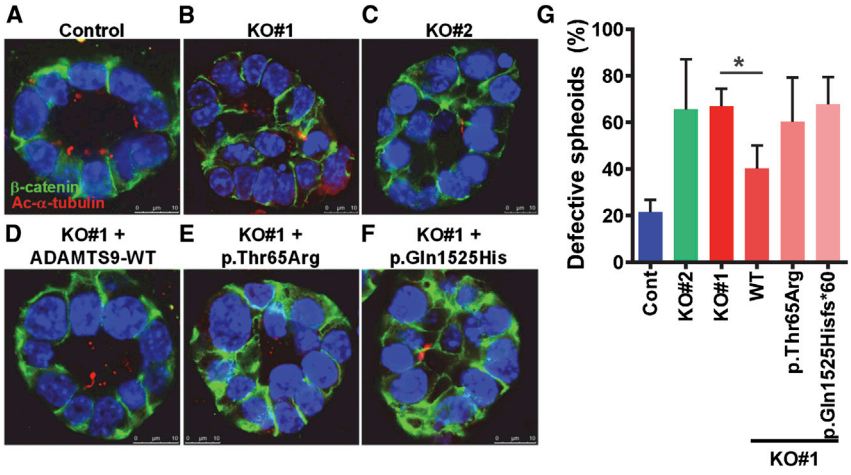

Figure 4. *Adamts9* Knockout Perturbs Lumen Formation in 3D Spheroid Culture
(A–F) IMCD3 cells are ciliated apically and form a spheroid containing a central lumen when cultured in 3D Matrigel. Lumen formation was perturbed in *Adamts9* knockout (KO) cells. Defective lumen formation was partially rescued by transfection with human wild-type (WT) *ADAMTS9* but not with *ADAMTS9* constructs harboring mutations detected in individuals with NPHP-RC. Cells were stained with anti-acetylated-α-tubulin (Ac-α-tubulin) and anti-β-catenin antibodies.
(G) Percentage of abnormal spheroids. More than 200 spheroids were examined in each experiment. Data represent the means ± standard deviation of five independent experiments. *$p < 0.05$, t test.

Adamts9$^{-/-}$ mice are embryonic lethal,[22] null mutations might result in Meckel-Gruber syndrome (MIM: 249000) or disease phenotypes that are incompatible with life. Therefore, the frameshift mutation detected in individual F1279-21 is unlikely to be functionally null but rather is likely to be a hypomorph because the resulting truncated protein would retain the intact metalloproteinase activity.

In this study, we showed that ADAMTS9 was present intracellularly near the base of the primary cilium during interphase. Because ADAMTS9 has a signal peptide and is conventionally transported through the endoplasmic reticulum to the Golgi apparatus and then to the extracellular space,[18] the intracellular localization of ADAMTS9 to the base of the cilium was unexpected. This localization seems to be important for the ciliary function of ADAMTS9; the mutant ADAMTS9 proteins detected in individuals with NPHP-RC failed to localize to the base of the primary cilium and also failed to rescue defects in lumen formation. In addition, because treatment of cells with an endocytosis inhibitor prevented exogenous ADAMTS9 from reaching the base of the cilium, we concluded that endocytosis was required for localization of ADAMTS9 near basal bodies. These findings suggest that secreted ADAMTS9 needs to be endocytosed in order for it to be localized near the basal body. Additional research is necessary to reveal the machinery involved in the endocytic

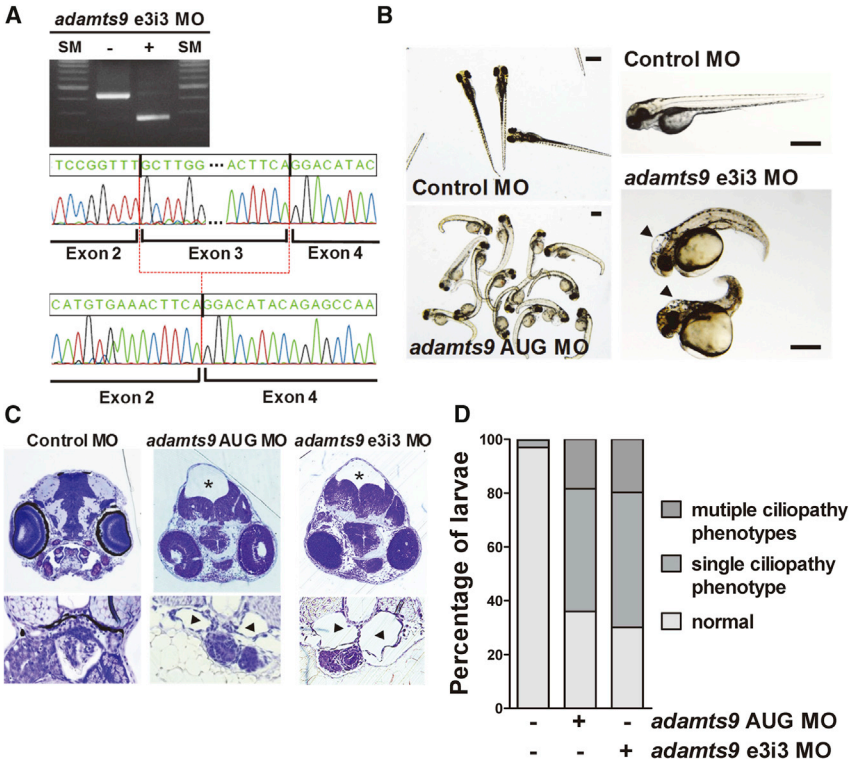

Figure 5. Knockdown of *adamts9* in Zebrafish Recapitulates Ciliopathy Phenotypes
(A) RT-PCR shows that injection of e3i3 splice-donor morpholino (MO) resulted in shortened *adamts9* mRNA compared to wild-type *adamts9* mRNA. A chromatogram of RT-PCR products revealed that exon 3 skipping was induced by e3i3 MO, resulting in the splicing of exons 2 and 4 (i.e., exon 3 deletion). SM = size marker.
(B) Compared to control-injected embryos, embryos injected with either *adamts9*-translation-blocking (AUG) or e3i3 MOs showed a ventrally bent body axis and hydrocephalus (arrowheads) at 3 days post-fertilization (dpf). The scale bar represents 1 mm.
(C) Methylene blue staining showed hydrocephalus (asterisks) or dilation of the pronephric duct (arrowheads) in *adamts9* morphants at 3 dpf.
(D) Summary of phenotypes of zebrafish morphants. More than 200 larvae were counted per condition.

mechanism of ADAMTS9 and elucidate the pathway by which it reaches primary cilia.

ADAMTS9 is a metalloprotease that regulates the structure and function of the extracellular matrix (ECM).[21] In this study, we found that the loss of ADAMTS9 resulted in shortened cilia and defective Shh signaling, but it is not clear whether the metalloproteinase activity of ADAMTS9 is required for its ciliary function. It is known that the ECM can affect primary cilia formation and function,[24] and renal cystogenesis is controlled by stromal composition;[25] therefore, it is plausible that shortened cilia might be due to ECM changes resulting from the loss of ADAMTS9. However, because we found that mutant ADAMTS9 proteins that retained the metalloproteinase domain were secreted into the medium to the same extent as wild-type protein, the ECM is unlikely to differ in individuals with *ADAMTS9* mutations. Rather, the intracellular function of ADAMTS9 near the basal body seems more relevant for primary-cilia function. However, it is not known whether ADAMTS9 detected near the basal body retains its metalloproteinase activity, and this also requires further investigation. In addition, there are 19 members in the human ADAMTS family.[21] ADAMTS9 belongs to the aggrecanase and proteoglycanase subgroup, which also includes ADAMTS1, 4, 5, 6, 15, and 20.[21] Thus, it will be interesting to examine whether any other ADAMTS proteins are involved in NPHP-RC.

Supplemental Data

Supplemental Data include five figures and one table and can be found with this article online at https://doi.org/10.1016/j.ajhg.2018.11.003.

Acknowledgments

The authors thank the families who contributed to this study. F.H. is the Warren E. Grupe professor. F.H. was supported by grants from the National Institutes of Health (DK076683, DK068306). H.Y.G. was supported by the Basic Science Research Program through the National Research Foundation of Korea (NRF), funded by the Korean government (MSIT 2018R1A2A3074572 and 2018R1A5A2025079). S.S.A. is supported by the Allen Distinguished Investigator Program, The Paul G. Allen Frontiers Group, the American Heart Association, and the NIH-NHLBI Program of Excellence in Glycoscience HL107147. S.N. is supported by the Mark Lauer Pediatric Research Grant. E.W. was supported by the Leopoldina Fellowship Program, German National Academy of Sciences Leopoldina (LPDS 2015-07). We thank Yonsei Advanced Imaging Center in cooperation with Carl Zeiss Microscopy and Electron Microscopy Core. We also thank Dr. Seok Jun Moon (Yonsei University College of Dentistry) for sharing the SMO-GFP RPE1 cells, and we thank Drs. Shyam Bihari Bansal and Vijay Kher (Kidney Institute, Medanta, the Medicity, India).

Declaration of Interests

Friedhelm Hildebrandt is a cofounder and on the scientific advisory board of Goldfinch Bio Inc. The other authors declare no competing interests.

Received: July 21, 2018
Accepted: November 9, 2018
Published: December 20, 2018

Web Resources

dbSNP, https://www.ncbi.nlm.nih.gov/SNP/
Ensembl Genome Browser, http://www.ensembl.org/
Exome Variant Server, http://evs.gs.washington.edu/EVS/
genome Aggregation Database (gnomAD), http://gnomad.broadinstitute.org/
Mutation Taster, http://www.mutationtaster.org/
Online Mendelian Inheritance in Man (OMIM), http://www.omim.org/
PolyPhen2, http://genetics.bwh.harvard.edu/pph2/
RefSeq, https://www.ncbi.nlm.nih.gov/RefSeq
Sorting Intolerant From Tolerant (SIFT), http://sift.jcvi.org
UCSC Human Genome Bioinformatics Browser, http://genome.ucsc.edu/

References

1. Hildebrandt, F., and Zhou, W. (2007). Nephronophthisis-associated ciliopathies. J. Am. Soc. Nephrol. *18*, 1855–1871.
2. Hildebrandt, F., Benzing, T., and Katsanis, N. (2011). Ciliopathies. N. Engl. J. Med. *364*, 1533–1543.
3. Braun, D.A., and Hildebrandt, F. (2017). Ciliopathies. Cold Spring Harb. Perspect. Biol. *9*, a028191.
4. Halbritter, J., Porath, J.D., Diaz, K.A., Braun, D.A., Kohl, S., Chaki, M., Allen, S.J., Soliman, N.A., Hildebrandt, F., Otto, E.A.; and GPN Study Group (2013). Identification of 99 novel mutations in a worldwide cohort of 1,056 patients with a nephronophthisis-related ciliopathy. Hum. Genet. *132*, 865–884.
5. Braun, D.A., Schueler, M., Halbritter, J., Gee, H.Y., Porath, J.D., Lawson, J.A., Airik, R., Shril, S., Allen, S.J., Stein, D., et al. (2016). Whole exome sequencing identifies causative mutations in the majority of consanguineous or familial cases with childhood-onset increased renal echogenicity. Kidney Int. *89*, 468–475.
6. Kruglyak, L., Daly, M.J., Reeve-Daly, M.P., and Lander, E.S. (1996). Parametric and nonparametric linkage analysis: A unified multipoint approach. Am. J. Hum. Genet. *58*, 1347–1363.
7. Strauch, K., Fimmers, R., Kurz, T., Deichmann, K.A., Wienker, T.F., and Baur, M.P. (2000). Parametric and nonparametric multipoint linkage analysis with imprinting and two-locus-trait models: Application to mite sensitization. Am. J. Hum. Genet. *66*, 1945–1957.
8. Gudbjartsson, D.F., Jonasson, K., Frigge, M.L., and Kong, A. (2000). Allegro, a new computer program for multipoint linkage analysis. Nat. Genet. *25*, 12–13.
9. Hildebrandt, F., Heeringa, S.F., Rüschendorf, F., Attanasio, M., Nürnberg, G., Becker, C., Seelow, D., Huebner, N., Chernin, G., Vlangos, C.N., et al. (2009). A systematic approach to mapping recessive disease genes in individuals from outbred populations. PLoS Genet. *5*, e1000353.
10. Gee, H.Y., Otto, E.A., Hurd, T.W., Ashraf, S., Chaki, M., Cluckey, A., Vega-Warner, V., Saisawat, P., Diaz, K.A., Fang, H., et al. (2014). Whole-exome resequencing distinguishes cystic kidney diseases from phenocopies in renal ciliopathies. Kidney Int. *85*, 880–887.

11. Halbritter, J., Diaz, K., Chaki, M., Porath, J.D., Tarrier, B., Fu, C., Innis, J.L., Allen, S.J., Lyons, R.H., Stefanidis, C.J., et al. (2012). High-throughput mutation analysis in patients with a nephronophthisis-associated ciliopathy applying multiplexed barcoded array-based PCR amplification and next-generation sequencing. J. Med. Genet. *49*, 756–767.
12. Giles, R.H., Ajzenberg, H., and Jackson, P.K. (2014). 3D spheroid model of mIMCD3 cells for studying ciliopathies and renal epithelial disorders. Nat. Protoc. *9*, 2725–2731.
13. Kim, J., Lee, J.E., Heynen-Genel, S., Suyama, E., Ono, K., Lee, K., Ideker, T., Aza-Blanc, P., and Gleeson, J.G. (2010). Functional genomic screen for modulators of ciliogenesis and cilium length. Nature *464*, 1048–1051.
14. Nandadasa, S., Nelson, C.M., and Apte, S.S. (2015). ADAMTS9-mediated extracellular matrix dynamics regulates umbilical cord vascular smooth muscle differentiation and rotation. Cell Rep. *11*, 1519–1528.
15. Corbit, K.C., Aanstad, P., Singla, V., Norman, A.R., Stainier, D.Y., and Reiter, J.F. (2005). Vertebrate smoothened functions at the primary cilium. Nature *437*, 1018–1021.
16. Wen, X., Lai, C.K., Evangelista, M., Hongo, J.A., de Sauvage, F.J., and Scales, S.J. (2010). Kinetics of hedgehog-dependent full-length Gli3 accumulation in primary cilia and subsequent degradation. Mol. Cell. Biol. *30*, 1910–1922.
17. Schueler, M., Braun, D.A., Chandrasekar, G., Gee, H.Y., Klasson, T.D., Halbritter, J., Bieder, A., Porath, J.D., Airik, R., Zhou, W., et al. (2015). DCDC2 mutations cause a renal-hepatic ciliopathy by disrupting Wnt signaling. Am. J. Hum. Genet. *96*, 81–92.
18. Somerville, R.P., Longpre, J.M., Jungers, K.A., Engle, J.M., Ross, M., Evanko, S., Wight, T.N., Leduc, R., and Apte, S.S. (2003). Characterization of ADAMTS-9 and ADAMTS-20 as a distinct ADAMTS subfamily related to Caenorhabditis elegans GON-1. J. Biol. Chem. *278*, 9503–9513.
19. Dubail, J., and Apte, S.S. (2015). Insights on ADAMTS proteases and ADAMTS-like proteins from mammalian genetics. Matrix Biol. *44–46*, 24–37.
20. Mead, T.J., and Apte, S.S. (2018). ADAMTS proteins in human disorders. Matrix Biol. *71–72*, 225–239.
21. Kelwick, R., Desanlis, I., Wheeler, G.N., and Edwards, D.R. (2015). The ADAMTS (A Disintegrin and Metalloproteinase with Thrombospondin motifs) family. Genome Biol. *16*, 113.
22. Dubail, J., Aramaki-Hattori, N., Bader, H.L., Nelson, C.M., Katebi, N., Matuska, B., Olsen, B.R., and Apte, S.S. (2014). A new Adamts9 conditional mouse allele identifies its non-redundant role in interdigital web regression. Genesis. *52*, 702–712.
23. Louie, C.M., Caridi, G., Lopes, V.S., Brancati, F., Kispert, A., Lancaster, M.A., Schlossman, A.M., Otto, E.A., Leitges, M., Gröne, H.J., et al. (2010). AHI1 is required for photoreceptor outer segment development and is a modifier for retinal degeneration in nephronophthisis. Nat. Genet. *42*, 175–180.
24. Seeger-Nukpezah, T., and Golemis, E.A. (2012). The extracellular matrix and ciliary signaling. Curr. Opin. Cell Biol. *24*, 652–661.
25. Cruz, N.M., Song, X., Czerniecki, S.M., Gulieva, R.E., Churchill, A.J., Kim, Y.K., Winston, K., Tran, L.M., Diaz, M.A., Fu, H., et al. (2017). Organoid cystogenesis reveals a critical role of microenvironment in human polycystic kidney disease. Nat. Mater. *16*, 1112–1119.